This is a repository copy of *Synergy between Ion Migration and Charge Carrier Recombination in Metal-Halide Perovskites*.

Article:

Synergy between Ion Migration and Charge Carrier Recombination in Metal-Halide Perovskites

SCHOLARONE™
Manuscripts

Synergy between Ion Migration and Charge Carrier Recombination in Metal-Halide Perovskites

Chuan-Jia Tong[1,2,3], Linqiu Li[2], Li-Min Liu[1]*, Oleg V. Prezhdo[2]*

[1]*School of Physics, Beihang University, Beijing 100191, China*
[2]*Department of Chemistry, University of Southern California, Los Angeles, California 90089, United States*
[3]*Department of Physics, University of York, Heslington, York YO10 5DD, United Kingdom*

Abstract: Charge carrier recombination plays a vital role in the $CH_3NH_3PbI_3$ perovskite solar cell. By investigating a possible synergy between ion migration and charge carrier recombination, we demonstrate that the nonradiative recombination accelerates by an order of magnitude during iodide migration. The migration induces lattice distortion that brings electrons and holes close to each other and increases their electrostatic interactions. The wave function localization in the same spatial region, and the enhanced lattice and iodide movements increase the nonadiabatic coupling. At the same time, quantum coherence lasts longer, because electron and hole energy levels become correlated. All these factors greatly increase the recombination rate. Moreover, the energy level of the iodide vacancy created during the migration moves from inside the conduction band in the equilibrated structure into the band gap, acting as a typical efficient nonradiative charge recombination center. Our work shows that the different dynamic processes are strongly correlated in halide perovskites, and demonstrates that defects, considered to be benign, can become very detrimental under non-equilibrium conditions. The reported results strongly suggest that ion migration should be avoided in halide perovskites, both for own reasons, such as large current-voltage hysteresis, and because it greatly accelerates charge carrier losses.

1. Introduction

Organic-inorganic halide perovskites, such as $CH_3NH_3PbI_3$ ($MAPbI_3$), are attracting considerable attention due to their exceptional optoelectronic properties, including high absorption coefficients with a sharp absorption edge, large charge carrier diffusion lengths, and high photoluminescence quantum efficiencies.[1-6] The last 10 years have witnessed a remarkable rise in the power conversion efficiency (PCE) of perovskite solar cells from 3.8 to 25.2%.[7,8] Despite the rapid progress, perovskites are still far from their full potential with further progress limited by losses of photogenerated charge carriers due to trapping and recombination.

Migration of ions, along with Schottky vacancies, constitutes a vital issue in perovskites, because it is the source of many unusual phenomena, such as the current-voltage hysteresis.[9-15] Multiple experimental and theoretical studies demonstrate that iodide is the most mobile ion.[16-21] It is well established that defects play detrimental roles in solar cell materials, because they act as traps and recombination centers that shorten charge carrier lifetimes.[22-24] It has been demonstrated that the defect state induced by the iodine vacancy is either located within the conduction band or forms a very shallow donor close to the conduction band minimum (CBM).[25-28] This conclusion implies that the iodine vacancy should not provide an efficient pathway for charge carrier relaxation in perovskites. Shallow defects are typically benign to carrier lifetime. Even if carrier recombination is accelerated by shallow defects, the acceleration is modest.[29] Recombination of trapped charges with the free complementary charge carriers can be even slower than recombination of the free carriers.[30] Then, transient trapping of charges by shallow defects can effectively extend charge carrier lifetimes, since the trapped charges escape back to the bands rather than recombine. However, recent works[31-38] suggest, directly or indirectly, that there may exist a synergy between charge carrier recombination and ion migration. For example, using steady-state and transient photoluminescence measurements, Kim et al.[32] found that surface-passivating ligands in perovskite nanoparticle films can prevent the ion migration, and at the same time, the passivated films show much reduced defect-related nonradiative recombination and improved photo-stability. Stranks[39] argued the importance of a fundamental understanding of the mechanisms of nonradiative losses and ion migration in perovskites for design of devices approaching their theoretical efficiency limits. Both experiment and theory indicate that charge carriers recombine in halide perovskites within nanoseconds.[30,40-42] Ion migration occurs on similar timescales. Azpiroz et al.[19] reported a 7.7×10^{10}

s^{-1} migration rate for two consecutive iodine hops with an energy barrier of 0.16 eV. Our previous work[43] showed the migration barrier of iodide can be as low as 0.06 eV for the most favorable orientation of the MA cations, and that the average barrier is around 0.3 eV, giving the migration rate is about 10^9 s^{-1}, according to the Arrhenius equation, $k = \frac{k_B T}{\hbar} e^{-\frac{Ea}{RT}}$. Since the charge recombination and ion migration can occur on similar timescales, it is necessary to establish whether these two very important processes influence each other.

In this work, we use time-domain first-principles simulations to investigate the synergy between iodide ion migration and electron-hole recombination in the MAPbI$_3$ perovskite. Our simulation shows that I$^-$ migration induces charge redistribution of the valence band maximum (VBM) and the conduction band minimum (CBM), which enhances the electron-hole overlap. The movement of I$^-$ and the associated lattice distortion produce a significantly increased nonadiabatic coupling (NAC). As a result, the electron-hole recombination is accelerated by an order of magnitude during the iodide migration. Moreover, when the iodide ion moves into the middle between two stable sites, the defect level induced by the corresponding iodine vacancy shifts downward into the band gap. The transiently created deep gap state acts as a typical nonradiative recombination center. During this time period, the electron-phonon interactions are the strongest, and the charge carrier losses are the fastest. The reported results demonstrate, for the first time, that ion migration can strongly promote nonradiative charge carrier recombination, indicating clearly that ion migration should be prevented in order to maximize the overall performance of perovskite solar cells.

2. Simulation Methodology

The first-principles molecular dynamics (FPMD) trajectories were calculated within the framework of density functional theory (DFT), as implemented in the CP2K/Quickstep package.[44] The valence electrons were described with Gaussian functions consisting of double-ζ polarized basis sets (m-DZVP)[45] and the core electrons were described with norm-conserving Goedecker-Teter-Hutter (GTH)[46] pseudopotentials. The energy cutoff for the real space grid was set as 500 Ry. A $2 \times 2 \times 2$ supercell (384 atoms) of the tetragonal unit cell was used in the whole study. Considering the practical computational cost for such a large cell, the exchange-correlation energy was calculated with the Perdew-Burke-Ernzerhof (PBE) functional[47] and the DFT-D3 description of van

der Waals interactions.[48,49] The PBE functional has performed well with nonadiabatic molecular dynamics (NAMD) calculations in MAPbI$_3$-type and even BaTiO$_3$-type perovskites.[50,51] Having generated FPMD trajectories using CP2K, we transferred them to VASP,[52] and generated Kohn-Sham orbitals and NAC that enter the NAMD calculations. NAMD were performed using the decoherence-induced surface hopping (DISH) approach,[53] which had been implemented in the PYXAID package.[54,55] The method has proven to be reliable in simulating excited state dynamics in other perovskite systems.[40,56-59] More theory details are shown in Supporting Information (SI).

3. Results and Discussion

3.1 Iodide diffusion

Figure 1a exhibits the initial MAPbI$_3$ structure with a uniform dipole polarization pointing up to the Z direction, as shown by colored triangles. As discussed in the previous work, the I$^-$ diffusion greatly depends on the dipole distribution of MA, and the lowest pathway is against the dipole direction of CH$_3$NH$_3$ (MA) cations (Figure 1b). The FPMD simulations (Figure 1c-f) show that iodide ion prefers to diffuse from parallel (P) site to the vicinity of vertical (V) site, against the dipole direction, agreeing well with the previous results.[43] The whole process lasts around 4500 fs and the movement of I$^-$ reaches around 5 Å. Meanwhile, an obvious configuration distortion including rotation of MA molecules and distortion of PbI$_2$ plane occurs along with the iodide migration. Especially, when I$^-$ moves into the middle area between P and V, the distortion reaches maximum. As shown in Figure 1d-e, the four PbI$_6$ octahedra adjacent to the migrated iodine all become totally irregular due to serious distortion. To quantify the distortion, we collect the distortion degree of these four octahedra during the whole migration process. Here, the distortion degree is defined as the average dispersion of four corresponding horizontal PbI$_2$ planes. Numerically speaking, it is the root-mean-square of Z coordinates of those Pb and I atoms who constitute the horizontal plane. The results are shown in Figure 2a. At first during t = 0 fs, the distortion degree is close to zero, which corresponds to a tiny structure distortion induced by iodine vacancy defect. As time going on, the increased distortion degree appears with the iodide migration. Two particularly high peaks can be observed at around 1900 and 3100 fs. At that time, the iodide ion probably locates at the middle area between P and V according to Figure 1d-e.
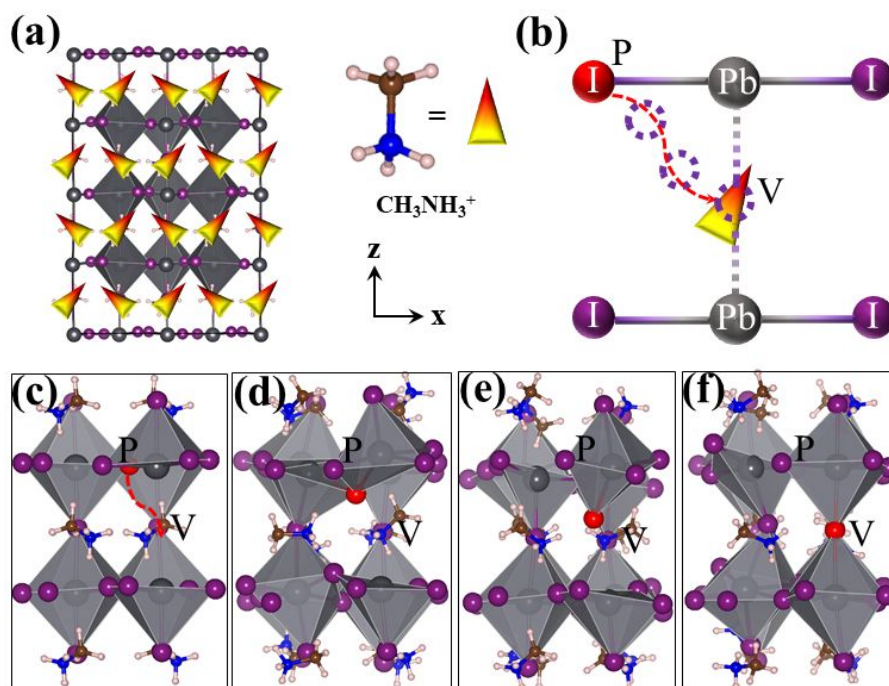
Figure 1 Relationship between I⁻ diffusion direction and the dipole distribution of MA⁺, as found in the first-principles molecules dynamics (FPMD) simulation. (a) Atomic structure of MAPbI$_3$ and the dipole distribution of MA⁺. (b) Schematic of I⁻ diffusion against the dipole direction of MA⁺; (c)-(f) The I⁻ diffusion as a function of the FPMD simulation times. Here, the selected snapshots (c), (d), (e) and (f) represent characteristic configurations during I⁻ diffusion at 0 fs, 1850 fs, 2800 fs, and 3350 fs, respectively. P and V represent stable parallel and vertical sites for the iodide ion. (Dark gray - lead; purple - iodine; red - migrated iodine; brown - carbon; blue - nitrogen; white - hydrogen)

To clearly trace the trajectory of migrated iodide ion, the distance between it and P/V site is plotted during the whole movement, as shown in Figure 2b. At the beginning, the iodide ion sets off from site P, which is about 4.29 Å away from site V of the destination. During the simulations, the distance between the iodide ion and site V (I-V, black line in Figure 2b) decreases with the increasing distance of I-P (red line). The cross point of two lines in Figure 2b indicates that the iodide ion reaches the geometric midpoint of P and V at the time of 2210 fs. In fact, during the period 1850~2800 fs, the iodide ion keeps moving at the vicinity around the midpoint, which can be also observed in Figure 1d-e. Moreover, the large slope of approximate linear displacement indicates the velocity of ion migration during this period is very large. Finally, it reaches the destination at around 3350 fs, and keeps wandering around V site with the fluctuation of no more

than 0.7 Å.

3.2 Influence of iodide diffusion on charge recombination

To explore how this migration behavior affects the electron-hole recombination between CBM and VBM, then the absolute NAC value along the whole diffusion process is carefully calculated as presented in Figure 2c. The NAC values are generally in meV scale, and the canonically averaged NAC value is 2.35 meV, much larger than that in pristine perovskite as reported in the previous works.[30,60] The larger NAC values indicate a probable faster charge carrier recombination occurs during iodide migration process. Besides, the NAC value reaches maximum (24.1 meV) at around 2 ps, and second maximum (22.7 meV) at around 3 ps. They are both very close to those two high peaks in the distortion degree curve (shown in Figure 2a), namely when iodide ion wandering around midpoint. It indicates there may be a relationship between strong distortion and large NAC, which has been confirmed in the following analysis. The NAC value is proportional to sensitivity of electronic wavefunctions to nuclear motion and to nuclear velocity. Both nuclear velocity and changes in electronic wavefunctions can be especially large when system's structure undergoes significant distortions. The unusually large NAC motivates us to explore the intrinsic reasons behind this phenomenon.
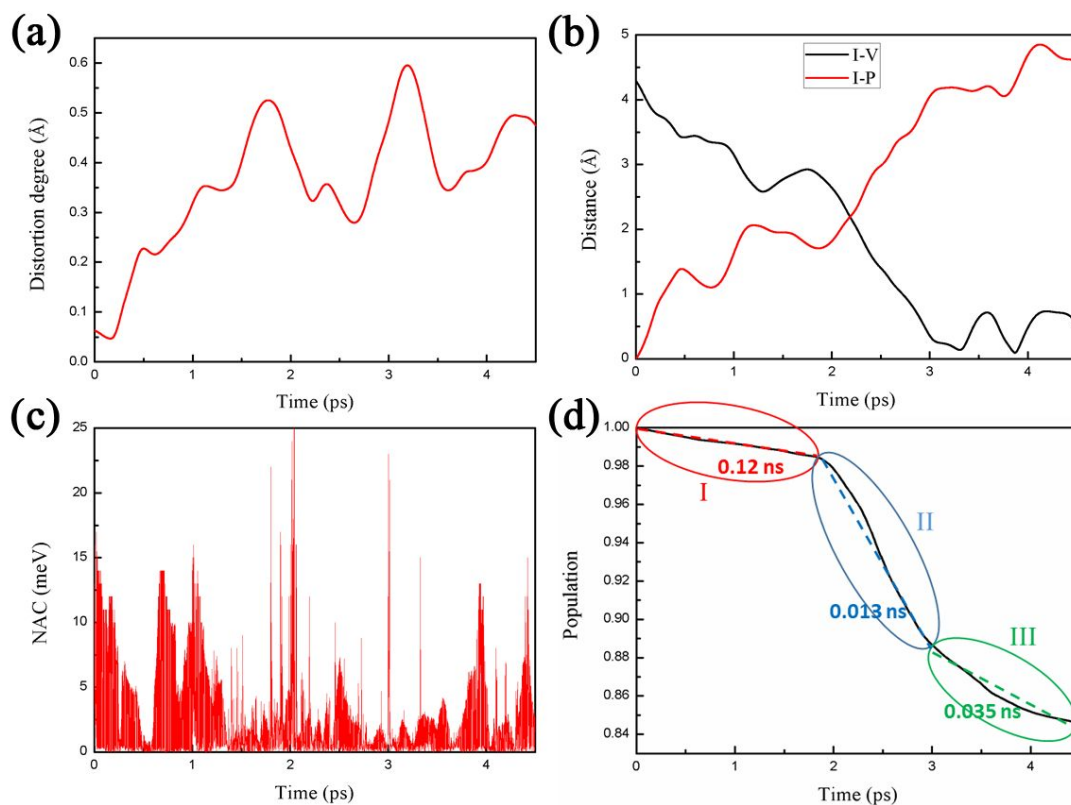
Figure 2. (a) The average degree of distortion of the four PbI_6 octahedra adjacent to the migrating iodine as shown in Figure 1c-f. (b) The distances from the iodide ion to site V (black line) and site P (red line) marked in Figure 1. (c) Time-dependent absolute NAC value during I^- migration. (d) Decay of the excited state population in the iodine-migrated perovskite due to the electron-hole recombination. The whole process is divided into three steps, I, II and III. The dashed lines show linear fits.

Figure 2d presents time evolution of population of the photo-excited state involved in the electron-hole recombination dynamics during the whole migration process. The population exhibits an abnormal stepwise decay, and it can be divided into three steps. Step I: from t = 0 to t = 1850 fs (highlighted in red in Figure 2d), it shows a smooth population decline (from 1 to 0.985). During this period, the iodide ion is moving from site P to the midpoint as discussed before. Step II: from t = 1850 to t = 2900 fs (highlighted in blue in Figure 2d), the population plummets from 0.985 to 0.889, much more rapidly than that in step I. During this period, the iodide ion experiences a very fast migration at the vicinity of the midpoint, with the maximum distortion of the lattice. Step III: from t = 2900 to t = 4500 fs (highlighted in green in Figure 2d), the population shows a mild decline

(from 0.889 to 0.844) compared with that in step II, but still faster than in step I. At this time, the iodide ion is mainly moving from the midpoint to site V and then wandering around it.

To determine the carrier recombination time, τ, for each step, we use the short-time linear approximation to the exponential decay, $f(t) = \exp(-t/\tau) \approx 1 - t/\tau$. The results are shown in dashed lines in Figure 2d. The fitted lines are shifted appropriately for steps II and III, to represent the initial time and population values for each stage, namely, for stage II, $y = 0.985 - (t-1850fs)/\tau$, and for stage III, $y = 0.889 - (t-2900fs)/\tau$. The relaxation time estimated for the nonradiative electron-hole recombination in iodine-migrated perovskite is 0.12 ns, 0.013 ns, 0.035 ns for step I, II, III, respectively (see in Figure 2d and Table 1). The shortest lifetime in step II tells us the electron-hole recombines the fastest when iodide ion moves around the midpoint of its migration. More importantly, the overall carrier lifetime scale here ($\sim 10^{-2}$ ns order) is far shorter than that in pristine perovskite ($\sim$ ns order), which means the benign iodine vacancy is not benign any more during the migration process. This conclusion agrees very well with many related experimental works,[31-33,37] suggesting that the ion diffusion could greatly speed up the electron-hole recombination. To further explore why the ion migration can accelerate the charge carrier recombination (schematically shown in Figure 3a), quantum coherence and electron-phonon interaction were calculated. In addition, we compare the results in the present I-vacancy (V_I) associated perovskite with those in pristine one.[60]

3.3 Analysis of electron-vibrational interactions

The pure-dephasing times, τ_d, are obtained using the optical response function formalism in the second order cumulant approximation to the pure-dephasing function[61], and fitting it by the Gaussian, $D(t) = \exp(-0.5(t/\tau_d)^2)$. Generally, loss of quantum coherence decreases transition rate, as exemplified by quantum Zeno effect.[62] The calculated pure-dephasing functions for both iodine-migrated and pristine perovskites are plotted in Figure 3b. The pure-dephasing in the perovskite is very fast due to the localized electrons and holes on different parts of the inorganic subsystem, Pb and I, respectively, and the small overlap between their wave functions. Therefore, the fitted pure-dephasing time in pristine perovskite is 3.29 fs, which is shorter than that in other semiconductors.[63,64] When iodide ion migrates in the perovskite, a slight slower quantum coherence loss occurs with a longer pure-dephasing time increasing into 6.15 fs (as shown in Figure 3b). This is probably attributed to the variation of charge distribution on VBM and CBM along with the ion

migration, confirmed by the following analysis. Anyhow, the slow decoherence rate contributes to a fast recombination and then a short carrier lifetime in iodine-migrated perovskite, which is also consistent with the NAMD result, as discussed above.

Table 1. Averaged pure-dephasing time, and nonradiative relaxation time for charge recombination during the three distinct steps in the iodine-migrated perovskite: I is prior to ion migration, II is during ion migration, III is after ion migration.

Step	dephasing time (fs)	relaxation time (ns)
I	5.23	0.12
II	6.07	0.013
III	6.36	0.035

Electron-phonon interaction is a key factor that could influence quantum dynamics of charge trapping and recombination. In order to characterize the phonon modes that couple to the electronic transitions between VBM and CBM, we calculate the autocorrelation functions of the electronic energy gaps and their Fourier transforms. The results are realized in the influence spectra as presented in Figure 3c. The intensity of each peak in the influence spectra shows the strength of electron-phonon coupling at the particular phonon frequency. As shown in Figure 3c, both iodine-migrated and pristine perovskite show dominant frequency modes around 100 cm^{-1} and 200 cm^{-1}. The lower frequency peaks should be assigned to inorganic Pb-I bending and stretching modes, in good agreement with the experimental results[65] (62 cm^{-1} and 90 cm^{-1}). It should be noted that high-frequency phonons are particularly important, because they have high velocities (for a given kinetic energy or temperature). The high frequency phonon could induce large NAC, which is proportional to the velocity. So the vibrational modes around 200 cm^{-1} should be assigned to much light MA cations, namely libration and torsional modes, as suggested by Raman spectrum.[65-67]

Compared the influence spectrum between the iodine-migrated and pristine perovskite in Figure 3c, several additional high frequency (> 400 cm^{-1}) peaks appear in iodine-migrated perovskite. These probably come from the fast movement of iodide ion and associated lattice distortion. Our previous work[60] has proved that the strong out-of-surface movement of whole MA molecules could

introduce additional high frequency modes, which strengthens the electron-phonon interaction. Here the movement of loose iodide ion is more intense, as it is not fully restricted by PbI_2 network now and its migration energy barrier is much lower than that of MA cations from previous publications[18,19]. Accordingly, these high frequency modes create larger NAC in iodine-migrated perovskite, which agrees well with the results as aforementioned. Combined with the longer decoherence rate, now we can clearly explain how ion migration accelerates the nonradiative electron-hole recombination in perovskite.
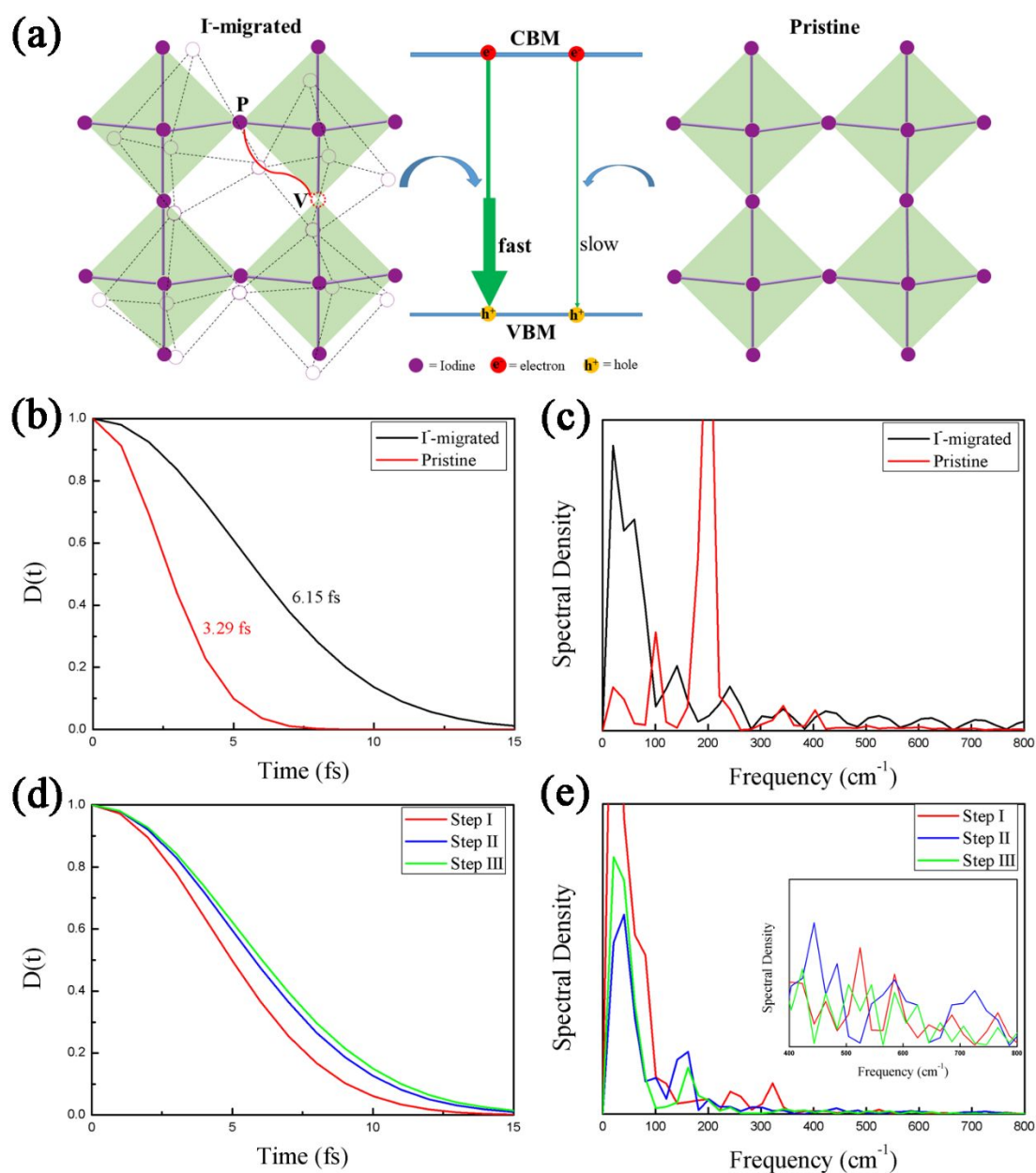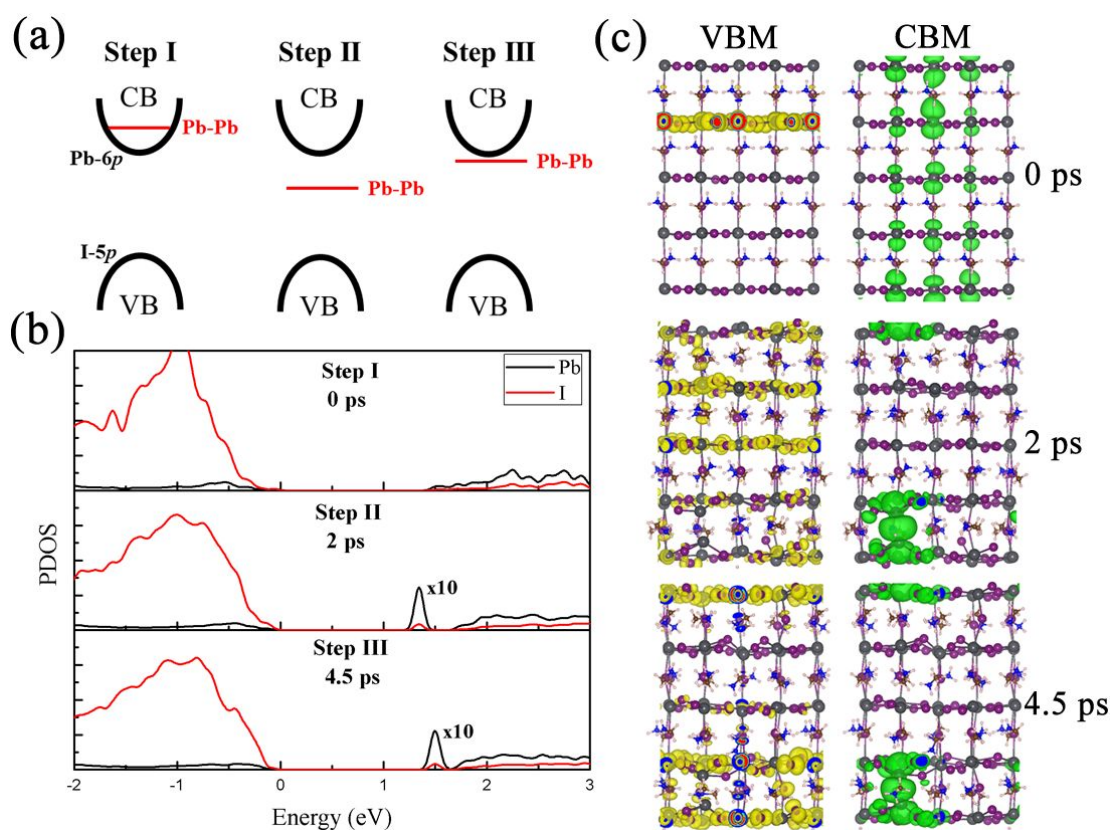

Figure 3. (a) Schematic diagram of electron-hole recombination in I⁻ migrated and pristine perovskites. Comparison of (b) pure-dephasing functions and (c) phonon influence spectra in I⁻

migrated and pristine perovskites. Comparison of (d) pure-dephasing functions and (e) phonon influence spectra for steps I, II and III marked in Figure 2 in I$^-$ migrated perovskite. The intensity scale of the spectral density in (e) is four times of that in (c). The insert in (e) shows the enlarged spectral density at higher frequencies.

To further figure out why there is a considerable difference in carrier lifetime between three steps during the iodide migration, we explore similar analyses on quantum coherence and electron-phonon interaction but separate them into three independent regions. The corresponding results are summarized in Figure 3d-e and Table I. Let's talk about the influence spectrum first. The dominant peaks near 100 cm^{-1} and 200 cm^{-1} can be observed in spectra of all three steps (Figure 3e). As above mentioned, additional high frequency (> 400 cm^{-1}) peaks play vital roles in iodine-migrated perovskite. When looking at high frequency area (400~800 cm^{-1}, insert in Figure 3e) between three steps, the main difference stems from that step II exhibits a relative larger intensity of spectral density during this area. As we have mentioned previously, when iodide ion migrates at the vicinity of the midpoint (namely step II), the velocity of the movement is very large and the distortion of the lattice reaches maximum. Therefore, the electron-phonon coupling interaction reaches maximum at this moment, which can well explain the shortest charge carrier lifetime in step II. As for step I and step III, the spectra densities are quite close in high frequency areas, a slightly lower than in step II, also in agreement with their longer carrier lifetimes than step II as shown in Figure 2d and Table 1.

When it comes to the quantum coherence, the pure-dephasing functions in Figure 3d clearly show that step I experiences the fastest coherence loss. Thus it has the shortest pure-dephasing time, 5.23 fs (see Table 1). Combined with relatively weak electron-phonon interaction, it can be realized that step I has the longest charge carrier lifetime among all three steps. By comparison, the pure-dephasing time in step III is the longest (6.36 fs), which indicates the transition rate from CBM to VBM should be higher than that in step I. As for step II, it exhibits a similar pure-dephasing function close to step III and its fitted dephasing time is 6.07 fs, slightly shorter than that in step III. So we can assume that the overlap of wave functions between the VBM and CBM should have little difference during step II and III.

Figure 4. (a) Schematic diagram of the iodine vacancy (V_I) defect level shift in the three different steps. (b) Projected density of states and (c) charge densities of the band edge states at t = 0, 2 and 4.5 ps.

3.4 Analysis of electronic structure

   In order to confirm our hypothesis, we select one representative trajectory for each step (t = 0 ps, t = 2 ps, t= 4.5 ps), and calculate their projected density of states (PDOS) and the charge densities of the corresponding VBM and CBM. When I⁻ starts to move at t = 0 ps, namely from site P (I-vacancy sits at site V), the defect state induced by V_I should locate inside the conduction band according to previous results as shown in Figure 4a. The PDOS (top panel in Figure 4b) confirms that no gap state is found at this moment and the partial charge density (top panel in Figure 4c) reveals that the CBM is mainly contributed by lead (Pb-6p orbitals) atoms, whereas the VBM is mainly contributed by part of iodine (I-5p orbitals) atoms. Similar as in pristine perovskite, the VBM and CBM orbitals are still spatially separated, and therefore, leading the small overlap and low recombination rate before iodide migration. No contribution of organic MA cations has been found at the band edge states.

When it comes to t = 2 ps (step II), namely I⁻ moving at the vicinity of the midpoint, the PDOS (middle panel in Figure 4b) shows an unexpected deep gap state appears around 1.30 eV above the VBM. The charge density (middle panel in Figure 4c) indicates this gap state is mainly dominated by two dangling Pb atoms (adjacent to the migrated iodide ion). This agrees well with previous reports[29,68,69] that a strong Pb-Pb dimer bond could result in a deep trap state below the CBM in perovskite. Compared with results in step I when t = 0 ps, we can deduce that the defect state induced by V_I will have a downward shift from the conduction band when the iodide ion is moving into a transition site. The deep trap state implies that once the benign defect V_I now converts into a serious nonradiative recombination center (schematically shown in Figure 4a). This can well explain a recent work by Gerhard et al.[37], a random switching is caused by ion diffusing which can passivate or activate a nonradiative center. And the reduced energy gap between two related orbitals can also explain the extraordinary large NAC values around 2 ps, as aforementioned in Figure 2c. In addition, except for dangling Pb atoms, their neighboring distorted iodine atoms also contribute some to gap state. In the meantime, the VBM is almost dominated by all iodine atoms. So the wave function overlap is larger than that in step I. That is why step II has a longer dephasing time than step I, as shown in Table 1.

After I⁻ reaching the destination and wandering around site V at t = 4.5 ps, the deep trap state proceeds an upward shift and becomes a shallow one (bottom panel in Figure 4b). But its charge distribution (bottom panel in Figure 4c) is almost the same as that in step II, which can also well explain their similar dephasing functions. The main change of charge density comes from the distribution at the VBM. At this time, the VBM is mainly contributed by those iodine atoms who are close to the migrated I⁻, with a large charge density. The spatial overlap of wave functions between VBM and CBM is the largest among all three steps, which results in the largest pure-dephasing time in step III. To quantify the intensity of the overlap, we calculated the overlap integral between VBM and CBM, which is defined as

$$\int |\Psi_{VBM}(r)||\Psi_{CBM}(r)|d^3r$$

Here, Ψ_i is the wave function of the ith orbital, which satisfies $\int |\Psi_i|^2 d^3r = 1$. Apparently, the overlap integral will be zero if the VBM and CBM charge densities are completely localized in separated regions. The calculated overlap integrals for t = 0, 2 and 4.5 ps are 0.011, 0.015 and 0.017,

respectively, following the same order as we analyze above. Meanwhile, step III exhibits the shallow defect level compared with step I, which should be the main reason for the shorter charge carrier lifetime than step I. But the charge carrier lifetime of step III is still longer than that of step II due to much weak electron-phonon interaction. In brief, the charge density redistribution of the VBM and CBM orbitals occurs along with the iodide ion migration, and the redistribution increases the overlap of wave functions, which slows down the quantum coherence loss, compared with the pristine perovskite as shown in Figure 3b.

Migration of the iodine vacancy is the most common type of defect migration, since the vacancy is one of the most stable native defects with low formation energy,[28,43] and the I$^-$ ion migration has a low migration barrier.[16-18,20] Migration of other defects and ions, such as Pb^{2+} and $CH_3NH_3^+$, can also influence charge carrier lifetimes in halide perovskites, and such synergy between ionic and charge motions deserves further investigation. Both I and Pb atoms contribute to the band edges, and therefore, their motions should have a strong effect on charge carrier properties. It would be interesting to see whether migration of $CH_3NH_3^+$ would accelerates the nonradiative charge recombination. Although $CH_3NH_3^+$ has no contribution to the band edges, its motions have proven to be detrimental to the carrier lifetimes by our previous work.[60] The current work focused on the neutral system, in which migration of the I$^-$ ion leaves a positively charged vacancy. It is the most important and widely studied case of iodine vacancy. It has been reported that a static positive iodine vacancy greatly accelerates charge recombination due to introduction of a deep trap state.[29] Studies of the influence of migration of defects in different oxidation states on charge recombination constitutes an important topic of further research.

4. Conclusions

In summary, using a combination of real-time TDDFT and NAMD, we have investigated the nonradiative electron-hole recombination during iodide migration in the now classic, $MAPbI_3$ perovskite. We demonstrated that the ion migration accelerates the charge recombination by nearly two orders of magnitude compared to the pristine system, and by an order of magnitude compared to the system immediately prior to the migration. The enhanced charge carrier losses are attributed to the following factors. *First*, the ion migration causes lattice distortions that localize electron and hole wavefunctions close to each other, enhancing electrostatic interactions between the charges.

Second, localization of the electron and hole wave functions in the same spatial region increases the NAC and prolongs the quantum coherence, both factors accelerating the nonradiative charge recombination. *Third*, the defect level of the iodide vacancy, created by the migrating iodide, moves inside the perovskite band gap during the migration processes and acts as a typical nonradiative recombination center, creating additional pathways for charge carrier losses.

The iodide migration process can be separated into three steps (I, II, III), immediately prior, during, and after the iodide migration. The carrier recombination rates for these steps are 8.3 ns^{-1}, 77 ns^{-1} and 29 ns^{-1}, respectively. The trap state of the iodide vacancy shift downward in energy from the conduction band into the band gap, ~1.3 eV above the VBM, when I^{-} reaches the transition state in step II, around the midpoint between the two stable sites. The mid-gap trap state acts as an efficient nonradiative recombination center by introducing smaller energy gaps and large NAC. Step II exhibits the strongest electron-phonon interactions because of the enhanced I^{-} movement and large lattice distortion during this period. The increased correlation between the electron and hole promotes slower quantum coherence loss in step III immediately after the migration, leading to a faster excited state population decay compared to step I before the migration. Finally, even though an equilibrated iodine vacancy may be benign for the nonradiative electron-hole recombination, the vacancy is very detrimental during its migration. This phenomenon has not been realized before and may apply to other defects as well. Our work suggests strongly that ion migration should be inhibited in perovskites, not only because it causes strong current-voltage hysteresis, but also since it greatly shortens charge carrier lifetimes. The in-depth understanding of the synergy between the ion migration and the charge recombination generated by our simulations assists in the development of high efficiency perovskite solar cells.

AUTHOR INFORMATION

Corresponding Authors

*E-mail: liminliu@buaa.edu.cn (L.-M.L.).

*E-mail: prezhdo@usc.edu (O.V.P.).

References

(1) Manser, J. S.; Christians, J. A.; Kamat, P. V. Intriguing Optoelectronic Properties of Metal Halide Perovskites. *Chem. Rev.* **2016**, *116*, 12956.

(2) Qin, P.; Paek, S.; Dar, M. I.; Pellet, N.; Ko, J.; Grätzel, M.; Nazeeruddin, M. K. Perovskite Solar Cells with 12.8% Efficiency by Using Conjugated Quinolizino Acridine Based Hole Transporting Material. *J. Am. Chem. Soc.* **2014**, *136*, 8516.

(3) Quarti, C.; Mosconi, E.; Ball, J. M.; D'Innocenzo, V.; Tao, C.; Pathak, S.; Snaith, H. J.; Petrozza, A.; De Angelis, F. Structural and Optical Properties of Methylammonium Lead Iodide across the Tetragonal to Cubic Phase Transition: Implications for Perovskite Solar Cells. *Energy Environ. Sci.* **2016**, *9*, 155.

(4) Hao, F.; Stoumpos, C. C.; Chang, R. P. H.; Kanatzidis, M. G. Anomalous Band Gap Behavior in Mixed Sn and Pb Perovskites Enables Broadening of Absorption Spectrum in Solar Cells. *J. Am. Chem. Soc.* **2014**, *136*, 8094.

(5) Tong, C.-J.; Geng, W.; Tang, Z.-K.; Yam, C.-Y.; Fan, X.-L.; Liu, J.; Lau, W.-M.; Liu, L.-M. Uncovering the Veil of the Degradation in Perovskite $CH_3NH_3PbI_3$ Upon Humidity Exposure: A First-Principles Study. *J. Phys. Chem. Lett.* **2015**, *6*, 3289.

(6) Zhumekenov, A. A.; Saidaminov, M. I.; Haque, M. A.; Alarousu, E.; Sarmah, S. P.; Murali, B.; Dursun, I.; Miao, X.-H.; Abdelhady, A. L.; Wu, T.; Mohammed, O. F.; Bakr, O. M. Formamidinium Lead Halide Perovskite Crystals with Unprecedented Long Carrier Dynamics and Diffusion Length. *ACS Energy Lett.* **2016**, *1*, 32.

(7) Kojima, A.; Teshima, K.; Shirai, Y.; Miyasaka, T. Organometal Halide Perovskites as Visible-Light Sensitizers for Photovoltaic Cells. *J. Am. Chem. Soc.* **2009**, *131*, 6050.

(8) https://www.nrel.gov/pv/assets/pdfs/best-research-cell-efficiencies.20190802.pdf.

(9) Son, D.-Y.; Kim, S.-G.; Seo, J.-Y.; Lee, S.-H.; Shin, H.; Lee, D.; Park, N.-G. Universal Approach toward Hysteresis-Free Perovskite Solar Cell Via Defect Engineering. *J. Am. Chem. Soc.* **2018**, *140*, 1358.

(10) Mosconi, E.; De Angelis, F. Mobile Ions in Organohalide Perovskites: Interplay of Electronic Structure and Dynamics. *ACS Energy Lett.* **2016**, *1*, 182.

(11) Yoon, S. J.; Draguta, S.; Manser, J. S.; Sharia, O.; Schneider, W. F.; Kuno, M.; Kamat, P. V. Tracking Iodide and Bromide Ion Segregation in Mixed Halide Lead Perovskites During Photoirradiation. *ACS Energy Lett.* **2016**, *1*, 290.

(12) Samu, G. F.; Balog, Á.; De Angelis, F.; Meggiolaro, D.; Kamat, P. V.; Janáky, C. Electrochemical Hole Injection Selectively Expels Iodide from Mixed Halide Perovskite Films. *J. Am. Chem. Soc.* **2019**, *141*, 10812.

(13) van Reenen, S.; Kemerink, M.; Snaith, H. J. Modeling Anomalous Hysteresis in Perovskite Solar Cells. *J. Phys. Chem. Lett.* **2015**, *6*, 3808.

(14) Richardson, G.; O'Kane, S. E. J.; Niemann, R. G.; Peltola, T. A.; Foster, J. M.; Cameron, P. J.; Walker, A. B. Can Slow-Moving Ions Explain Hysteresis in the Current-Voltage Curves of Perovskite Solar Cells? *Energy Environ. Sci.* **2016**, *9*, 1476.

(15) Chen, R.; Cao, J.; Duan, Y.; Hui, Y.; Chuong, T. T.; Ou, D.; Han, F.; Cheng, F.; Huang, X.; Wu, B.; Zheng, N. High-Efficiency, Hysteresis-Less, UV-Stable Perovskite Solar Cells with Cascade ZnO–ZnS Electron Transport Layer. *J. Am. Chem. Soc.* **2019**, *141*, 541.

(16) Yuan, Y.; Huang, J. Ion Migration in Organometal Trihalide Perovskite and Its Impact on

Photovoltaic Efficiency and Stability. *Acc. Chem. Res.* **2016**, *49*, 286.

(17) Yuan, Y.; Wang, Q.; Shao, Y.; Lu, H.; Li, T.; Gruverman, A.; Huang, J. Electric-Field-Driven Reversible Conversion between Methylammonium Lead Triiodide Perovskites and Lead Iodide at Elevated Temperatures. *Adv. Energy Mater.* **2016**, *6*, 1501803.

(18) Eames, C.; Frost, J. M.; Barnes, P. R. F.; O'Regan, B. C.; Walsh, A.; Islam, M. S. Ionic Transport in Hybrid Lead Iodide Perovskite Solar Cells. *Nat. Commun.* **2015**, *6*, 7497.

(19) Azpiroz, J. M.; Mosconi, E.; Bisquert, J.; De Angelis, F. Defect Migration in Methylammonium Lead Iodide and Its Role in Perovskite Solar Cell Operation. *Energy Environ. Sci.* **2015**, *8*, 2118.

(20) Haruyama, J.; Sodeyama, K.; Han, L.; Tateyama, Y. First-Principles Study of Ion Diffusion in Perovskite Solar Cell Sensitizers. *J. Am. Chem. Soc.* **2015**, *137*, 10048.

(21) Yang, J.-H.; Yin, W.-J.; Park, J.-S.; Wei, S.-H. Fast Self-Diffusion of Ions in $CH_3NH_3PbI_3$: The Interstiticaly Mechanism Versus Vacancy-Assisted Mechanism. *J. Mater. Chem. A* **2016**, *4*, 13105.

(22) Li, W.; Long, R.; Tang, J.; Prezhdo, O. V. Influence of Defects on Excited-State Dynamics in Lead Halide Perovskites: Time-Domain Ab Initio Studies. *J. Phys. Chem. Lett.* **2019**, *10*, 3788.

(23) Yoon, S. J.; Kuno, M.; Kamat, P. V. Shift Happens. How Halide Ion Defects Influence Photoinduced Segregation in Mixed Halide Perovskites. *ACS Energy Lett.* **2017**, *2*, 1507.

(24) Landi, G.; Neitzert, H. C.; Barone, C.; Mauro, C.; Lang, F.; Albrecht, S.; Rech, B.; Pagano, S. Correlation between Electronic Defect States Distribution and Device Performance of Perovskite Solar Cells. *Advanced Science* **2017**, *4*, 1700183.

(25) Yin, W.-J.; Shi, T.; Yan, Y. Unusual Defect Physics in $CH_3NH_3PbI_3$ Perovskite Solar Cell Absorber. *Appl. Phys. Lett.* **2014**, *104*, 063903.

(26) Mosconi, E.; Meggiolaro, D.; Snaith, H. J.; Stranks, S. D.; De Angelis, F. Light-Induced Annihilation of Frenkel Defects in Organo-Lead Halide Perovskites. *Energy Environ. Sci.* **2016**, 3180.

(27) Kim, J.; Lee, S.-H.; Lee, J. H.; Hong, K.-H. The Role of Intrinsic Defects in Methylammonium Lead Iodide Perovskite. *J. Phys. Chem. Lett.* **2014**, *5*, 1312.

(28) Meggiolaro, D.; De Angelis, F. First-Principles Modeling of Defects in Lead Halide Perovskites: Best Practices and Open Issues. *ACS Energy Lett.* **2018**, *3*, 2206.

(29) Li, W.; Sun, Y.-Y.; Li, L.; Zhou, Z.; Tang, J.; Prezhdo, O. V. Control of Charge Recombination in Perovskites by Oxidation State of Halide Vacancy. *J. Am. Chem. Soc.* **2018**, *140*, 15753.

(30) Li, W.; Liu, J.; Bai, F.-Q.; Zhang, H.-X.; Prezhdo, O. V. Hole Trapping by Iodine Interstitial Defects Decreases Free Carrier Losses in Perovskite Solar Cells: A Time-Domain Ab Initio Study. *ACS Energy Lett.* **2017**, *2*, 1270.

(31) deQuilettes, D. W.; Zhang, W.; Burlakov, V. M.; Graham, D. J.; Leijtens, T.; Osherov, A.; Bulović, V.; Snaith, H. J.; Ginger, D. S.; Stranks, S. D. Photo-Induced Halide Redistribution in Organic–Inorganic Perovskite Films. *Nat. Commun.* **2016**, *7*, 11683.

(32) Kim, Y.-H.; Wolf, C.; Kim, H.; Lee, T.-W. Charge Carrier Recombination and Ion Migration in Metal-Halide Perovskite Nanoparticle Films for Efficient Light-Emitting Diodes. *Nano Energy* **2018**, *52*, 329.

(33) Tress, W.; Yavari, M.; Domanski, K.; Yadav, P.; Niesen, B.; Correa Baena, J. P.; Hagfeldt, A.; Graetzel, M. Interpretation and Evolution of Open-Circuit Voltage, Recombination, Ideality Factor and Subgap Defect States During Reversible Light-Soaking and Irreversible Degradation of Perovskite Solar Cells. *Energy Environ. Sci.* **2018**, *11*, 151.

(34) Calado, P.; Telford, A. M.; Bryant, D.; Li, X.; Nelson, J.; O'Regan, B. C.; Barnes, P. R. F. Evidence for Ion Migration in Hybrid Perovskite Solar Cells with Minimal Hysteresis. *Nat. Commun.* **2016**, *7*,

13831.

(35) Nandal, V.; Nair, P. R. Predictive Modeling of Ion Migration Induced Degradation in Perovskite Solar Cells. *ACS Nano* **2017**, *11*, 11505.

(36) Sherkar, T. S.; Momblona, C.; Gil-Escrig, L.; Ávila, J.; Sessolo, M.; Bolink, H. J.; Koster, L. J. A. Recombination in Perovskite Solar Cells: Significance of Grain Boundaries, Interface Traps, and Defect Ions. *ACS Energy Lett.* **2017**, *2*, 1214.

(37) Gerhard, M.; Louis, B.; Camacho, R.; Merdasa, A.; Li, J.; Kiligaridis, A.; Dobrovolsky, A.; Hofkens, J.; Scheblykin, I. G. Microscopic Insight into Non-Radiative Decay in Perovskite Semiconductors from Temperature-Dependent Luminescence Blinking. *Nat. Commun.* **2019**, *10*, 1698.

(38) Walsh, A.; Stranks, S. D. Taking Control of Ion Transport in Halide Perovskite Solar Cells. *ACS Energy Lett.* **2018**, *3*, 1983.

(39) Stranks, S. D. Nonradiative Losses in Metal Halide Perovskites. *ACS Energy Lett.* **2017**, *2*, 1515.

(40) Liu, L.; Fang, W.-H.; Long, R.; Prezhdo, O. V. Lewis Base Passivation of Hybrid Halide Perovskites Slows Electron–Hole Recombination: Time-Domain Ab Initio Analysis. *J. Phys. Chem. Lett.* **2018**, *9*, 1164.

(41) Xing, G.; Mathews, N.; Sun, S.; Lim, S. S.; Lam, Y. M.; Grätzel, M.; Mhaisalkar, S.; Sum, T. C. Long-Range Balanced Electron- and Hole-Transport Lengths in Organic-Inorganic $CH_3NH_3PbI_3$. *Science* **2013**, *342*, 344.

(42) Li, Y.; Yan, W.; Li, Y.; Wang, S.; Wang, W.; Bian, Z.; Xiao, L.; Gong, Q. Direct Observation of Long Electron-Hole Diffusion Distance in $CH_3NH_3PbI_3$ Perovskite Thin Film. *Sci. Rep.* **2015**, *5*, 14485.

(43) Tong, C.-J.; Geng, W.; Prezhdo, O. V.; Liu, L.-M. Role of Methylammonium Orientation in Ion Diffusion and Current–Voltage Hysteresis in the $CH_3NH_3PbI_3$ Perovskite. *ACS Energy Lett.* **2017**, *2*, 1997.

(44) VandeVondele, J.; Krack, M.; Mohamed, F.; Parrinello, M.; Chassaing, T.; Hutter, J. Quickstep: Fast and Accurate Density Functional Calculations Using a Mixed Gaussian and Plane Waves Approach. *Comput. Phys. Commun.* **2005**, *167*, 103.

(45) VandeVondele, J.; Hutter, J. Gaussian Basis Sets for Accurate Calculations on Molecular Systems in Gas and Condensed Phases. *J. Chem. Phys.* **2007**, *127*, 114105.

(46) Goedecker, S.; Teter, M.; Hutter, J. Separable Dual-Space Gaussian Pseudopotentials. *Phys. Rev. B* **1996**, *54*, 1703.

(47) Perdew, J. P.; Burke, K.; Ernzerhof, M. Generalized Gradient Approximation Made Simple. *Phys. Rev. Lett.* **1996**, *77*, 3865.

(48) Grimme, S.; Antony, J.; Ehrlich, S.; Krieg, H. A Consistent and Accurate Ab Initio Parametrization of Density Functional Dispersion Correction (DFT-D) for the 94 Elements H-Pu. *J. Chem. Phys.* **2010**, *132*, 154104.

(49) Grimme, S.; Ehrlich, S.; Goerigk, L. Effect of the Damping Function in Dispersion Corrected Density Functional Theory. *J. Comput. Chem.* **2011**, *32*, 1456.

(50) Li, W.; Zhang, X.; Lu, G. Unraveling Photoexcitation Dynamics at "Dots-in-a-Perovskite" Heterojunctions from First-Principles. *J. Mater. Chem. A* **2019**, *7*, 18012.

(51) Lian, C.; Ali, Z. A.; Kwon, H.; Wong, B. M. Indirect but Efficient: Laser-Excited Electrons Can Drive Ultrafast Polarization Switching in Ferroelectric Materials. *J. Phys. Chem. Lett.* **2019**, *10*, 3402.

(52) Kresse, G.; Furthmüller, J. Efficient Iterative Schemes for Ab Initio Total-Energy Calculations Using a Plane-Wave Basis Set. *Phys. Rev. B* **1996**, *54*, 11169.

(53) Jaeger, H. M.; Fischer, S.; Prezhdo, O. V. Decoherence-Induced Surface Hopping. *J. Chem. Phys.*

2012, *137*, 22A545.

(54) Akimov, A. V.; Prezhdo, O. V. The PYXAID Program for Non-Adiabatic Molecular Dynamics in Condensed Matter Systems. *J. Chem. Theory Comput.* **2013**, *9*, 4959.

(55) Akimov, A. V.; Prezhdo, O. V. Advanced Capabilities of the PYXAID Program: Integration Schemes, Decoherence Effects, Multiexcitonic States, and Field-Matter Interaction. *J. Chem. Theory Comput.* **2014**, *10*, 789.

(56) Long, R.; Liu, J.; Prezhdo, O. V. Unravelling the Effects of Grain Boundary and Chemical Doping on Electron–Hole Recombination in $CH_3NH_3PbI_3$ Perovskite by Time-Domain Atomistic Simulation. *J. Am. Chem. Soc.* **2016**, *138*, 3884.

(57) Jankowska, J.; Prezhdo, O. V. Ferroelectric Alignment of Organic Cations Inhibits Nonradiative Electron–Hole Recombination in Hybrid Perovskites: Ab Initio Nonadiabatic Molecular Dynamics. *J. Phys. Chem. Lett.* **2017**, *8*, 812.

(58) Zhang, Z.; Fang, W.-H.; Tokina, M. V.; Long, R.; Prezhdo, O. V. Rapid Decoherence Suppresses Charge Recombination in Multi-Layer 2D Halide Perovskites: Time-Domain Ab Initio Analysis. *Nano Lett.* **2018**, *18*, 2459.

(59) He, J.; Fang, W.-H.; Long, R.; Prezhdo, O. V. Superoxide/Peroxide Chemistry Extends Charge Carriers' Lifetime but Undermines Chemical Stability of $CH_3NH_3PbI_3$ Exposed to Oxygen: Time-Domain Ab Initio Analysis. *J. Am. Chem. Soc.* **2019**, *141*, 5798.

(60) Tong, C.-J.; Li, L.; Liu, L.-M.; Prezhdo, O. V. Long Carrier Lifetimes in PbI_2-Rich Perovskites Rationalized by Ab Initio Nonadiabatic Molecular Dynamics. *ACS Energy Lett.* **2018**, *3*, 1868.

(61) Akimov, A. V.; Prezhdo, O. V. Persistent Electronic Coherence Despite Rapid Loss of Electron–Nuclear Correlation. *J. Phys. Chem. Lett.* **2013**, *4*, 3857.

(62) Kilina, S. V.; Neukirch, A. J.; Habenicht, B. F.; Kilin, D. S.; Prezhdo, O. V. Quantum Zeno Effect Rationalizes the Phonon Bottleneck in Semiconductor Quantum Dots. *Phys. Rev. Lett.* **2013**, *110*, 180404.

(63) Li, L.; Long, R.; Prezhdo, O. V. Charge Separation and Recombination in Two-Dimensional MoS_2/WS_2: Time-Domain Ab Initio Modeling. *Chem. Mater.* **2017**, *29*, 2466.

(64) Li, L.; Long, R.; Bertolini, T.; Prezhdo, O. V. Sulfur Adatom and Vacancy Accelerate Charge Recombination in MoS_2 but by Different Mechanisms: Time-Domain Ab Initio Analysis. *Nano Lett.* **2017**, *17*, 7962.

(65) Quarti, C.; Grancini, G.; Mosconi, E.; Bruno, P.; Ball, J. M.; Lee, M. M.; Snaith, H. J.; Petrozza, A.; Angelis, F. D. The Raman Spectrum of the $CH_3NH_3PbI_3$ Hybrid Perovskite: Interplay of Theory and Experiment. *J. Phys. Chem. Lett.* **2014**, *5*, 279.

(66) Pérez-Osorio, M. A.; Milot, R. L.; Filip, M. R.; Patel, J. B.; Herz, L. M.; Johnston, M. B.; Giustino, F. Vibrational Properties of the Organic–Inorganic Halide Perovskite $CH_3NH_3PbI_3$ from Theory and Experiment: Factor Group Analysis, First-Principles Calculations, and Low-Temperature Infrared Spectra. *J. Phys. Chem. C* **2015**, *119*, 25703.

(67) Niemann, R. G.; Kontos, A. G.; Palles, D.; Kamitsos, E. I.; Kaltzoglou, A.; Brivio, F.; Falaras, P.; Cameron, P. J. Halogen Effects on Ordering and Bonding of $CH_3NH_3^+$ in $CH_3NH_3PbX_3$ (X = Cl, Br, I) Hybrid Perovskites: A Vibrational Spectroscopic Study. *J. Phys. Chem. C* **2016**, *120*, 2509.

(68) Kim, J.; Chung, C.-H.; Hong, K.-H. Understanding of the Formation of Shallow Level Defects from the Intrinsic Defects of Lead Tri-Halide Perovskites. *Phys. Chem. Chem. Phys.* **2016**, *18*, 27143.

(69) Uratani, H.; Yamashita, K. Charge Carrier Trapping at Surface Defects of Perovskite Solar Cell Absorbers: A First-Principles Study. *J. Phys. Chem. Lett.* **2017**, *8*, 742.

1
2
3
4
5
6
7
8
9
10
11
12
13
14
15
16
17
18
19
20
21
22
23
24
25
26
27
28
29
30
31
32
33
34
35
36
37
38
39
40
41
42
43
44
45
46
47
48
49
50
51
52
53
54
55
56
57
58
59
60

Table of Content Graphic